Arabian Journal of Chemistry (2019) **12**, 3753–3763

King Saud University

Arabian Journal of Chemistry

www.ksu.edu.sa
www.sciencedirect.com

ORIGINAL ARTICLE

Ceria–zirconia solid solution loaded hierarchical MFI zeolite: An efficient catalyst for solvent free oxidation of ethyl benzene

Mithun Nandi, Anup Kumar Talukdar *

Department of Chemistry, Gauhati University Guwahati, Assam 781014, India

Received 3 December 2015; accepted 24 January 2016
Available online 29 January 2016

KEYWORDS

MFI;
Hierarchic MFI;
Ceria–zirconia;
Calcination temperature;
Ethyl benzene

Abstract Hierarchical MFI supported ceria–zirconia solid solution was synthesized following de position–precipitation method at different calcination temperatures. The structure and surface properties were analysed using XRD, TEM, DRS-UV–vis, SEM, nitrogen adsorption–desorption techniques. The as-synthesized samples were found to exhibit excellent catalytic activity for the oxidation of ethyl benzene by tert-butylhydroperoxide with excellent selectivity for acetophenone. Among the supported ceria–zirconia samples, the one calcined at 923 K demonstrated well-defined crystallites with (1 1 1) being the most exposed facets and showed highest activity under the optimized reaction conditions. A first order kinetics was observed for the reaction with a rate constant of 2.53×10^{-2} min^{-1} and activation energy of 21 kJ mol^{-1}. The catalyst was resistant to leaching and retained its activity even after the fifth run. The use of solvent in the reaction system was avoided to maintain a green protocol for the reaction.

1. Introduction

The advantages of ceria–zirconia solid solution (CZ) over pure CeO_2 or ZrO_2 include high thermal resistance, enhanced reduction efficiency of Ce^{4+}/Ce^{3+} redox couple and excellent oxygen storage/release capacity (OSC) (Kozlov et al., 2002). It also exhibits acid sites that originate due to different charge to radius ratio of Zr and Ce (Sugiura et al., 2005). Hu and group carried out the esterification of butanol and acetic acid over CZ and noticed high yield of butyl acetate in just 15 min of reaction time (Hu et al., 2008). Solinas and co-workers studied the dehydration of 4-methylpentan-ol to 4-methylpent-1-ene over the unsupported CZ. Though satisfactory results were obtained, the catalyst lacked thermal stability and was susceptible to sintering (Solinas et al., 2003). The same reaction was investigated by Reddy et al. with silica supported CZ that resulted with good activity and selectivity including high durability than the unsupported one (Reddy et al., 2006). The nature of support played a fundamental role on the physicochemical and catalytic properties of CZ. Because of excellent stability, high specific surface area, and excellent physical strength, microporous MFI and other zeolites have been extensively used as catalyst supports (Corma, 1997). However, the sole microporous nature may impose diffusion limitations in reactions involving bulky species. Intensive synthetic attempts have been made for several years to improve the accessibility and mass transport to

* Corresponding author.
E-mail address: guchem.talukdar@gmail.com (A.K. Talukdar).
Peer review under responsibility of King Saud University.

Production and hosting by Elsevier

http://dx.doi.org/10.1016/j.arabjc.2016.01.010
1878-5352

the active site for effective utilization of the zeolite as heterogeneous catalyst. Hierarchical zeolite combines the unique property of microporosity with complementary mesopore network of inter/intra crystalline nature (Thibault-Starzyk et al., 2009). The results of preliminary studies have shown that mordenite and ferrite required extreme alkali treatment to induce extra porosity and this results in generation of large pores. In contrast zeolite β is highly susceptible to mesopore formation even under very mild conditions (Groen et al., 2004). Faujasite type of zeolite contains supercages due to which faujasite deactivates faster than MFI zeolite. In addition, advantage of creating hierarchical MFI by desilication is that it results in the formation of combined micro and mesoporous materials with high degree of tunable porosity. A detailed study on hierarchical MFI based on our previous work revealed the improved pore architecture with enhanced mesopore volume and pore diameter (Kalita and Talukdar, 2011). The optimum conditions obtained in this study for alkali treatment of MFI zeolite have been utilized in the present investigation. To the best of our knowledge limited works have been carried out utilizing alkali treated MFI as catalyst support and no work has been reported on synthesis and use of ceria–zirconia solid solution supported on MFI zeolite. Recently Ogunronbi and co-workers have reported the advantages of hierarchical nature of Ga loaded ZSM-5 zeolite for propane aromatization (Ogunronbi et al., 2015). The nature of crystallite size is indeed an important factor to understand the catalytic properties of supported metal oxides. Recently, oxidation catalysts are receiving major attention because of their key role in chemicals production and also in the destruction of undesired products by total oxidation. A selective oxidative derivative of ethyl benzene (EB) is of much importance for the synthesis of value added products. Acetophenone is an oxidative product of EB that serves as a raw material in the production of perfumes, drugs, resins and pharmaceuticals (Alcántara et al., 2000; Ghiaci et al., 2010). The industrial production of acetophenone involves the oxidation of EB with molecular oxygen catalysed by homogenous cobalt catalysts (cobalt acetate or cobalt cycloalkane carboxylate), bromide species as promoter and acetic acid as solvent (Partenheimer, 1995). Despite its utility, the difficulty in separation and recovery and easy deactivation confine its large-scale practical industrial applications. Heterogeneous catalysts such as Mn/MCM-41 (Parida and Dash, 2009), Mn/APO-11, V/APO-11, Cr-MCM-41 (Singh et al., 1999), CeAPO-5 molecular sieves (Devika et al., 2011), Co/HMS (Bhoware et al., 2006) and some other Mn and Co containing complexes supported on alumina or silica (Arshadi and Giachi, 2011) were found to be active for the reaction. Therefore, the investigation for development of a highly efficient and environmentally benign catalyst that would overcome the limitations of leaching and at the same time that could be recovered and recycled is still of great interest.

In this present work, we report the preparation of hierarchical MFI supported ceria–zirconia solid solution by deposition–precipitation technique at different calcination temperatures ranging between 753 and 1073 K to correlate the effect of crystallite size and the catalytic activity. The as-synthesized samples were employed for the oxidation of EB with TBHP and found to be highly active with excellent selectivity towards acetophenone. The kinetics of the reaction was also studied and activation energy was determined. A green synthetic route was followed avoiding the use of any solvent. Recycling of the catalyst for at least five times was done with retention of its catalytic activity.

2. Experimental

2.1. Synthesis of hierarchical MFI

Studies have shown that a high aluminium content (low Si/Al ratio of about 15) stabilizes the surrounding silicon atoms to a high degree. Consequently, relatively small fraction of materials gets dissolved in alkali solution leading to hardly any or small pores in lower nanometer size. On the other hand, low framework aluminium concentration (high Si/Al ratio of about 1000) allows leaching of large portions for the zeolite crystal thereby inducing large pores. These large pores contribute much less to the required mesoporosity (Groen et al., 2006). That is why MFI zeolite with moderate Si/Al ratio (i.e. 100) is synthesized in the present study. For crystallization of a sample of parent MFI with silica to alumina ratio (SAR) 100, hydrothermal technique was adopted following our previously reported method under autogenous pressure (Kalita and Talukdar, 2009). The calcined product (UZ100) was subjected to alkali treatment with 0.4 M NaOH solution for a period of 60 min. 150 mL aqueous solution of 0.4 M NaOH solution was heated to 343 K in a polyethylene beaker placed in a water bath. To the pre-heated solution 2 g of parent MFI was introduced and set under constant stirring at the same temperature. The slurry was immediately cooled down in an ice-bath to prevent further reactions. The suspension was then filtered and the solid sample was washed several times with deionized water till all the alkali got removed. The product was dried overnight at ambient temperature and then at 383 K in an air oven for 6 h. The resulting desilicated sample is designated as DZ100.

2.2. Preparation of supported solid solution

The effect of initial composition of ceria and zirconia in CZ solid solution has been studied by Kenevey et al. According to their study for a $Ce_{0.5}Zr_{0.5}O_2$ solid solution, during calcination the tetragonal phase undergoes demixing, resulting in the creation of a ceria rich and zirconia rich compositions. Moreover, they have reported that throughout the advancement of the calcination this composition is maintained and no material with intermediate compositions is formed (Kenevey et al., 2001). That is why ceria and zirconia with Ce:Zr = 1:1 M ratio were supported on the modified MFI (DZ100) following dep osition–precipitation method using ammonium hydroxide solution as hydrolysing agent. 0.051 g of ammonium ceric nitrate (Rankem) and 0.030 g of zirconyl nitrate (Loba Chemie GR grade) were individually dissolved in deionized water and finally mixed together. To the homogenous solution 1 g of finely powdered DZ100 was added and stirred for 2 h. Aqueous ammonium hydroxide solution was added dropwise with constant stirring until precipitation was complete. The resulting precipitate was filtered, washed several times to remove the excess alkali, dried at 383 K for 6 h and finally calcined at 753 (CZD480), 923 (CZD650) and 1073 K (CZD800) in a muffle furnace. Scheme 1 depicts the schematic representation of catalyst preparation.

2.3. Catalytic oxidation of ethyl benzene

Catalytic oxidation of ethyl benzene (EB) was carried out with 70% tert-butyl hydroperoxide (TBHP) in a 25 mL reaction flask equipped with a water condenser. Various parameters such as the reactant molar ratio, temperature, amount of catalyst and reaction time were optimized maintaining the total volume of reactants at 5 mL for each run. The catalyst was preheated at 383 K for 3 h before every use. The progress of the reaction was monitored by withdrawing the reaction mixture after definite intervals of time and analysed by gas chromatography (Bruker 430 GC) fitted with WCOT fused silica

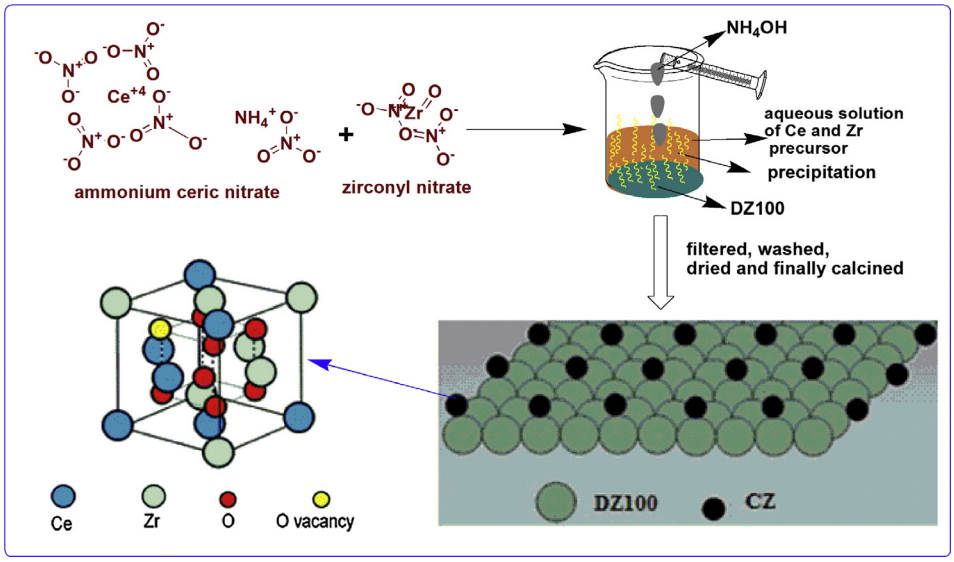

Scheme 1 Schematic representation for preparation of the catalyst.

30 m × 0.32 mm column and FID detector. The identities of the products were confirmed by comparing with the authentic sample. The conversion and selectivity were calculated from the gas chromatography data by the following equations:

$$\%\text{EB conversion} = [(\text{Mole EB}_{\text{inlet}} - \text{Mole EB}_{\text{outlet}})/\text{Mole EB}_{\text{inlet}}] \times 100 \quad (1)$$

$$\%\text{Selectivity of product (P1)} = [\text{Moles of P1/total moles of all products}] \times 100 \quad (2)$$

2.4. Characterization of the samples

Powdered X-ray diffraction patterns were recorded on a Bruker D-8 Advance X-ray diffractometer operated at 40 kV and 40 mA using Ni-filtered Cu Kα (0.15418 nm). The intensity data were collected over a 2θ range 5–80° with step size 0.05° and using counting time of 1 s. The surface morphology of the samples was obtained by a Hitachi, S-3600 N scanning electron microscope. Hitachi 4100 spectrometer equipped with a diffuse reflectance attachment was used to study the diffuse reflectance UV–vis spectra of the samples in the range 200–800 nm. Transmission electron microscopy (TEM) images were recorded on a JEOL 2011 electron microscope. For high resolution electron microscopy a suspension of the material in ethanol was placed in an ultrasound bath. A drop of it was placed on a carbon grid and the solvent was allowed to evaporate. The particles that remained on the walls of the grid were studied. The surface area and pore size measurement were done on a Micromeritics Tristar 3000 surface area and porosity analyser by nitrogen physisorption at liquid nitrogen temperature.

3. Results and discussion

3.1. X-ray diffraction analysis

X-ray diffraction patterns for ceria–zirconia solid solution supported on MFI samples are shown in Fig. 1. In addition to the well resolved peaks and prominent reflections of MFI characteristic lines, diffraction lines due to CZ solid solution were

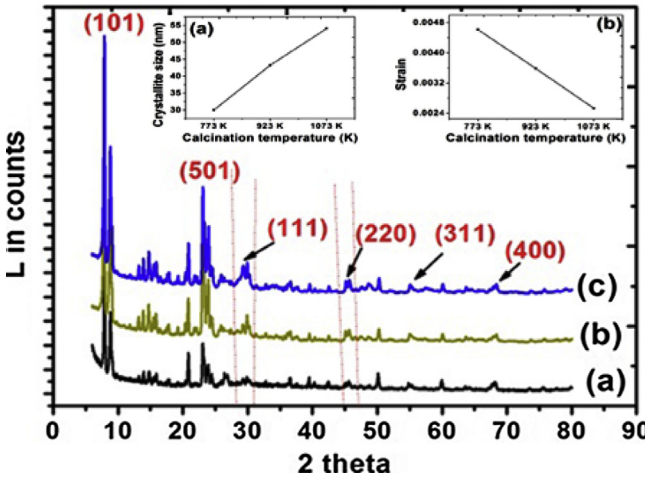

Figure 1 XRD pattern of (a) CZD480, (b) CZD650, (c) CZD800. Inset shows variation of (a) crystallite size and (b) strain with the calcination temperature.

also observed. The prominent peaks at 2θ = 7–9° and 23° correspond to characteristic peaks for MFI indicating formation of pure ZSM-5 phase (Treacy and Higgins, 2001). As reported in our earlier works alkaline treatment of MFI up to 90 min did not lead to any significant changes in the basic structure (Kalita and Talukdar, 2011). The observed XRD line patterns for CZ are found to be similar to those of CeO_2 with only slight shifting of the 2θ values (Reddy and Lakshmanan, 2005). The diffraction peaks at 2θ = 29.8°, 46°, 55.4° and 68.8° can be assigned to (1 1 1), (2 2 0), (3 1 1) and (4 0 0) planes respectively of CZ (Fig. 1) and characteristic cubic phase with fluorite structure (PDF-ICDD 28-0271). With increase in calcination temperature the intensity of lines pertaining to the cubic phases of CZ becomes more prominent. The tetragonal phase (2 2 0) for zirconia at 2θ = 50.3° was preserved in each case which is in agreement with Damayanova et al. that zirconia preserves its tetragonal phase under any composition of CZ depending on the fact that they contain a number of defects due to strong interactions with ceria sites (Damyanova et al.,

2008). Crystallite size is a measure of the size of coherently diffracting domain. The crystallite size was calculated using Williamson and Hall plot (Fig. 2) for deconvoluting size and strain broadening. The simplified equation in the Lorentzian peak shape is as follows:

$$\beta_{hkl}\cos\theta = \frac{K}{D} + 4\varepsilon sin\theta$$

where D is average crystallite size, K is a dimensionless shape factor with a value close to unity, λ is the wavelength of Cu Kα1 radiation (0.15406 nm), β_{hkl} is the line broadening at half the maximum intensity (FWHM) in radian and θ_{hkl} is Bragg angle in radian. The additional term ε denotes the average strain. Williamson and Hall plot is obtained by plotting $\beta\cos\theta$ against $4\sin\theta$. The crystallite size was calculated from the intercept of the linear fit. Crystallinity of the samples was determined using the following relation:

$$\%C = \frac{I_{hkl}}{I_b + I_{hkl}}$$

for a particular crystallographic plane (hkl) where, I_b is the integral background intensity and I_{hkl} is the integral peak intensity with reference to (1 0 1) and (5 0 1) planes. The results are presented in Table 1.

The strain (ε) was obtained from the slope of the plot. It is clearly observed that with the increase in the calcination temperature from 753 to 1073 K the strain associated with the samples decreased with increase in the crystallite size (Fig. 1, inset).

3.2. TEM analysis

To ascertain the observations obtained from XRD analysis and to investigate the structural evolution at atomic scale, TEM analysis was carried out for the three samples. The

Table 1 Crystallite size, strain and crystallinity from XRD analysis.

Sample	Crystallite size (nm)	Crystallinity (%)	Strain
CZD480	30	72	0.0046
CZD650	43	88	0.0035
CZD800	54	97	0.0025

TEM image of CZD480 (Fig. 3a) shows the particles to be homogenously dispersed on the zeolite surface. Further increase in the temperature to 923 then to 1073 K leads to larger particles with distinct crystallites (Fig. 3b and c). It is clearly observed from the TEM images that the increase in the calcination temperature is accompanied by a change in the morphology of the crystallites from irregular to spherical. The selected area diffraction pattern (SAED) for the different samples is shown in Fig. 3. Increase in temperature generates more ordered ring patterns accompanied with bright spots indicating enhanced crystallinity. The results are in good parity with the XRD data. The d-spacing value of about 0.31 nm for all the samples corresponds to (1 1 1) planes of CZ phase with fluorite structure and is the dominant exposed facets on the surface (Colon et al., 1999).

The histogram of particle size distribution at 753 K ranges from 2 to 4.5 nm centred around 4 nm (Fig. 3, inset). Similarly, the distributions at 923 and 1073 K centred about 7 and 11 nm respectively complementing the XRD results that with increase in the calcination temperature there is a significant increase in the particle size. Increase in the calcination temperature might lead to rapid rate of nucleation and increase in the supersaturation of the reaction products might accelerate the crystal core formation reaction (Parra and Haque, 2014).

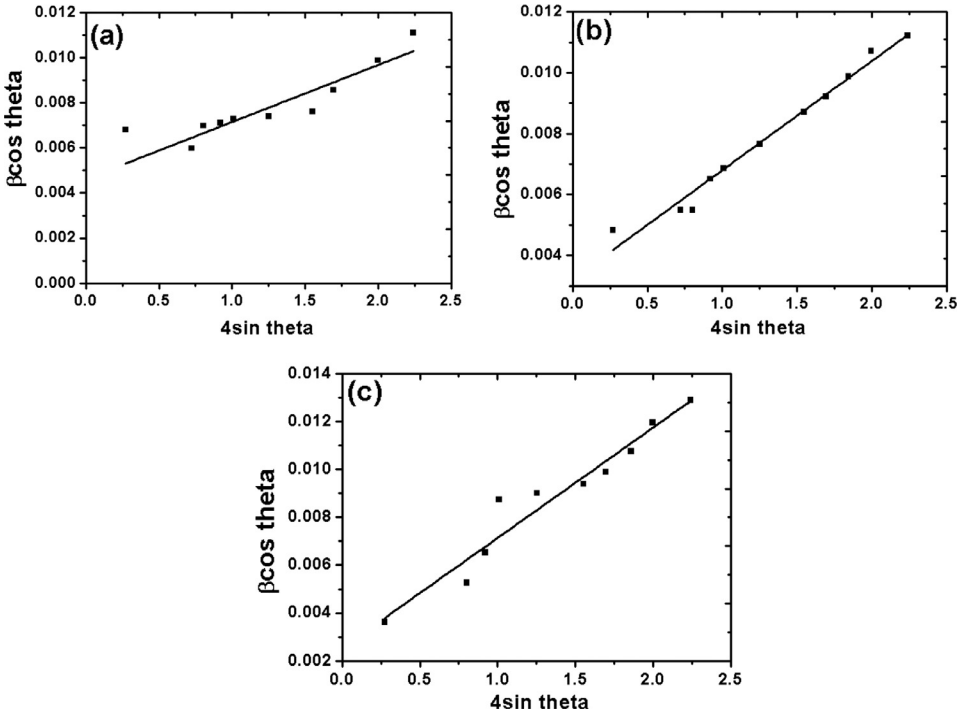

Figure 2 Williamson and Hall plot for (a) CZD480, (b) CZD650, (c) CZD800.

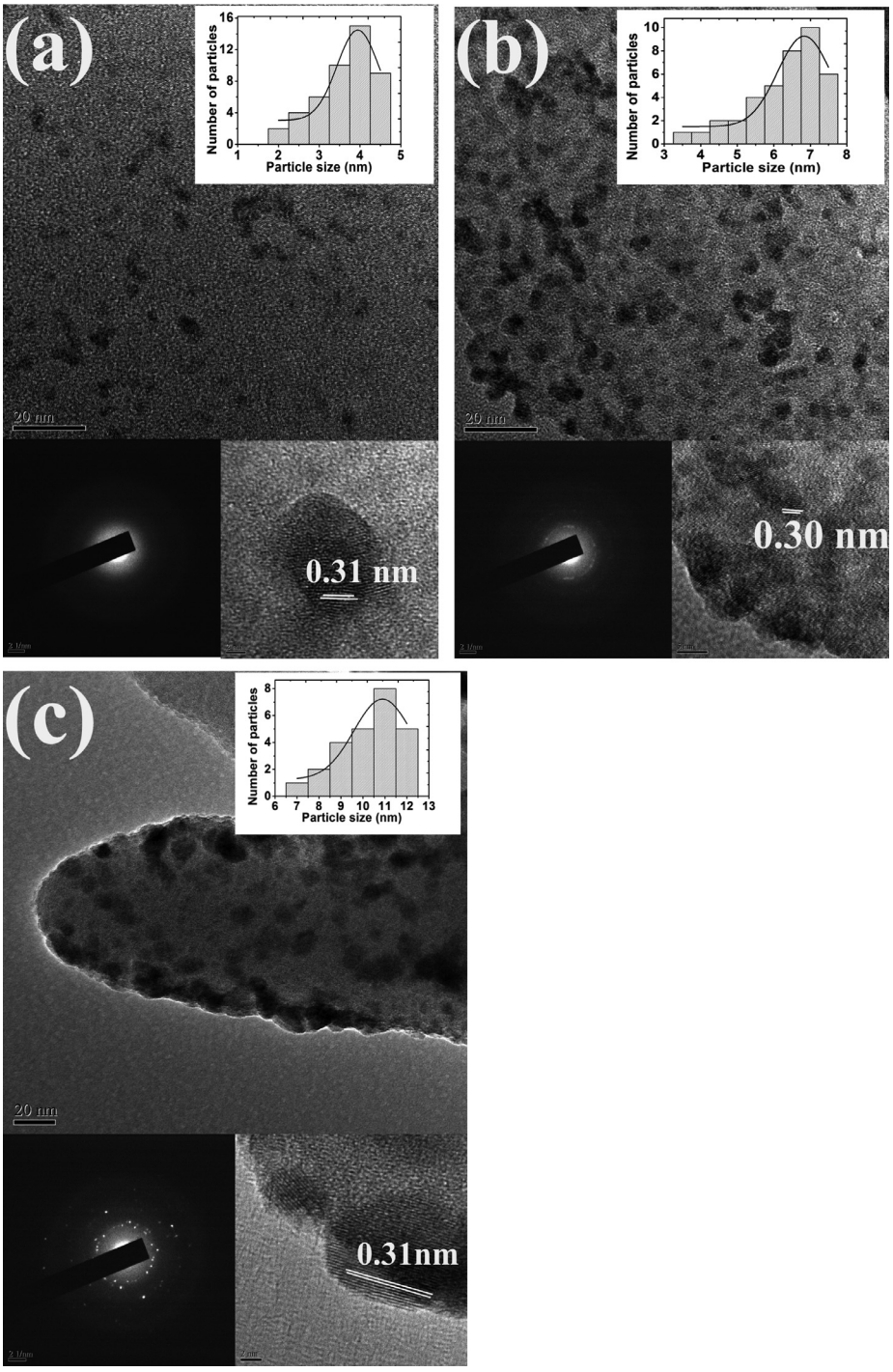

Figure 3 TEM, SAED image and lattice fringe of (a) CZD480, (b) CZD650, (c) CZD800. The inset in each case represents the histogram of particle size distribution for the respective sample.

3.3. SEM analysis

SEM micrograph for CZD650 is shown in Fig. 4. It can be seen that uniform and twinned cuboidal MFI particles were formed. The particles show uniform morphology with particle size in the range 20–25 μm. The elemental composition of the same sample was obtained from energy dispersive X-ray spectroscopy (EDX) analysis which indicates that CZD650 is composed of only Ce and Zr in addition to Si, Al and O (Fig. 4). No evidence of any impurities was observed and the formed solid solution was near to our expected stoichiometry (Table 2).

3.4. Surface area analysis

Fig. 5 illustrates the nitrogen adsorption–desorption isotherm of the parent and modified MFI samples. Prior to analysis all the samples were degassed for 4 h to remove any pre-adsorbed

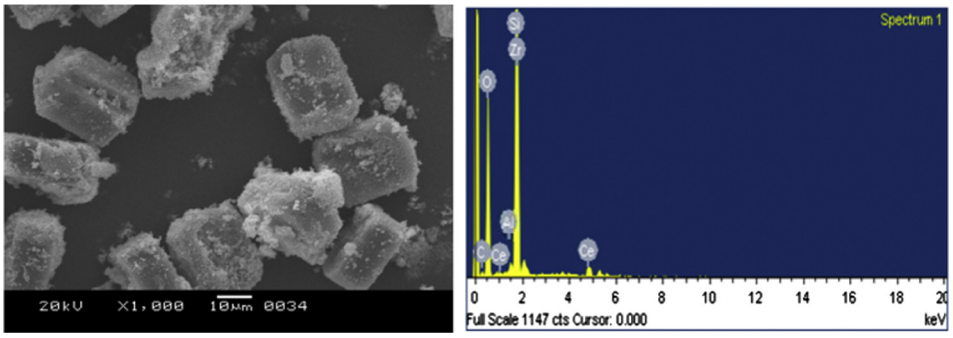

Figure 4 SEM and EDX analysis of CZD650.

gaseous species. The as-synthesized UZ100 seems to exhibit a type 1 isotherm with high up-taking at relatively low pressure indicating its microporous nature (Perry and Green, 1997). Upon alkali treatment for at least 60 min a typical combination of type-I and type-IV isotherms with H3 hysteresis loop is observed (Caicedo-Realpe and Perez-Ramirez, 2010; Perez-Ramirez et al., 2008). The desilicated MFI and the CZ samples at different calcination temperatures exhibit two hysteresis curves suggesting the presence of two mesopores sizes (Kalita and Talukdar, 2011). The capillary condensation loop at p/p_0 = 0.1–0.20 represents the mesoporosity confined in the framework and the prominent H3 type hysteresis loop in the higher partial pressure range (p/p_0 = 0.42–1.0) is characteristic of considerable amount of secondary mesopores originated from intercrystalline voids in the arrangement of crystals (Chen et al., 1997). The surface area and the pore volume decreased upon loading of CZ and are found to depend on the calcination temperature (Table 3). The decrease in surface area may be due to penetration of the impregnated oxides into the composite pores of the zeolite thereby reducing the pore volume (Reddy et al., 1997). Increase in the calcination temperature leads to bigger crystallites as evidenced from XRD (Table 1) and TEM analysis and the occupancy of these bigger crystallites on the pores might have decreased the pore volume.

3.5. UV–vis diffused reflectance spectroscopy

UV–vis DR spectroscopy has been used extensively to analyse ceria-based materials and transition metal oxides to gain information of different oxidation states of metal ions and surface co-ordinations by measuring d-d, f-d transitions and oxygen-metal ion charge transfer bands. Fig. 6 depicts the UV–vis DR spectra of CZ samples calcined at different temperatures ranging from 753 to 1073 K. The observed absorption bands are in the range 200–400 nm. The DRS pattern for all the samples can be resolved into four bands 220, 250, 290 and 335 nm. The band at 220 nm may be assigned to 4f-5d transitions due to $Ce^{3+} \rightarrow Zr^{4+}$. This seems to weaken with the increase in the calcination temperature of the samples indicating more involvement of Zr^{4+} in the solid solution (Rao and Sahu, 2001). The UV–vis band at 250 and 290 nm may be assigned to $Ce^{3+} \leftarrow O^{2-}$ and $Ce^{4+} \leftarrow O^{2-}$ charge transfer transitions respectively (Bensalem et al., 1995). The broad band in the range 320–350 nm may be assigned to interband transition and also $Zr^{4+} \leftarrow O^{2-}$ transition of the substituted fluorite structure. The broad band may be the characteristic of the solid solution that replaces two intense DRS features due to ceria and zirconia. This is in agreement with the explanation proposed by Bensalem (Bensalem et al., 1992) and Rao and Sahu (2001) for mechanical mixture of ceria and zirconia.

Table 2 Elemental composition of CZD650 as obtained from EDX analysis.

Elements	Atomic%
O	70.8
Al K	0.3
Si K	26.4
ZrL	1.3
CeL	1.2
Total	100

4. Catalytic activity

The catalytic activity of ceria–zirconia (CZ) loaded hierarchical MFI samples was investigated for the oxidation of ethyl benzene using TBHP as oxidant. The major product analysed was acetophenone (P1) together with benzaldehyde (P2) and benzoic acid (P3) as minor products. The reaction pathway is shown in Scheme 2. The blank reaction yielded only 5% conversion of EB after 4 h of reaction time and the conversion was same with parent and alkali treated MFI samples (Fig. 7). However, supported CZ solid solutions calcined at different temperatures were found to be highly active under similar reaction conditions. The conversions with CZD480 and CZD650 were 60% and 78% respectively. With CZD800, the conversion fell to 71%. The results are summarized in Table 4. The effect of different parameters was studied employing CZD650 catalyst to obtain an optimum condition for the reaction.

In order to evaluate the effect of temperature on the catalytic activity, the reaction was carried out in the temperature range 323–363 K. It is observed (Fig. 8) that with the rise in temperature, conversion of EB increased considerably up to 353 K after 4 h of reaction time. The selectivity towards acetophenone also increased (88%) with increase in the temperature till 353 K. However, increasing the temperature to 363 K the selectivity to P1 was found to decrease with simultaneous increase in the selectivities to P2 and P3. This may be due to heterolytic cleavage of C–C bond (of $-CH_2CH_3$) at elevated temperatures facilitating the rise in rate of formation of

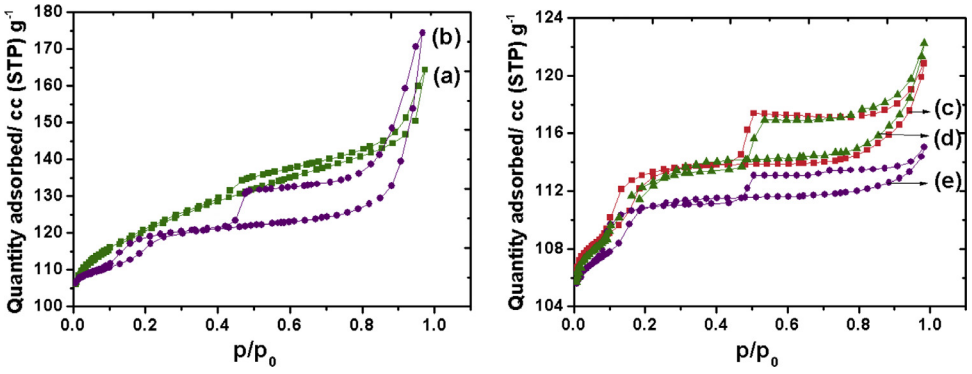

Figure 5 Nitrogen adsorption–desorption isotherm of (a) UZ100, (b) DZ100, (c) CZD480, (d) CZD650, (e) CZD800.

Table 3 Surface area and pore volume of the prepared samples.

Sample	[a]S_{BET} ($m^2\ g^{-1}$)	[b]V_{meso} ($cm^3\ g^{-1}$)	[c]V_T ($cm^3\ g^{-1}$)	[d]V_{micro} ($cm^3\ g^{-1}$)
UZ100	378	0.06	0.31	0.25
DZ100	418	0.25	0.42	0.17
CZD480	370	0.20	0.35	0.15
CZD650	362	0.18	0.32	0.14
CZD800	327	0.14	0.26	0.12

[a] BET surface area.
[b] Mesopore volume ($V_T - V_{micro}$).
[c] Total pore volume.
[d] Micropore volume obtained by *t*-plot.

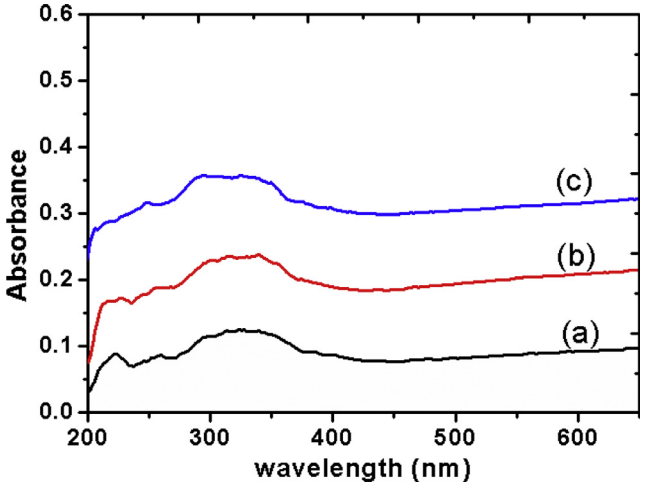

Figure 6 UV–vis DR spectra of (a) CZD480, (b) CZD650 (shifted by 0.13 units), (c) CZD800 (shifted by 0.24 units). Shifting is done for clarity.

benzaldehyde and benzoic acid (Xie et al., 2015). Therefore 353 K can be considered as the optimized temperature for the present oxidation reaction.

The influence of catalyst amount in the oxidation of EB is depicted in Fig. 9. The conversion of EB seems to improve with increase in the dosage of catalyst from 0.05 to 0.2 g. It is observed that with 0.05 g of catalyst amount only 40% of EB was converted. The conversion increased to 78% on increasing the catalyst amount to 0.1 g; the selectivity to acetophenone also increased from 70% to 88%. However, further increase in the catalyst amount to 0.2 g led only to a minimal increase in the conversion with decrease in the selectivity of P1. The excess active sites resulting from the increase in catalyst amount might easily adsorb the formed acetophenone which is further oxidized to benzaldehyde and benzoic acid. Taking into account both the conversion and selectivity 0.1 g can be considered to be the adequate amount of the catalyst for the reaction.

In order to investigate the influence of EB:TBHP molar feed ratio the reaction was performed with different molar ratios (1:1, 1:2, 2:1, 1:3 and 1:4) at 353 K for 4 h. The results are depicted in Fig. 10. It is clearly seen that the conversion of EB increased considerably with increase in the amount of oxidant. With 1:1 M ratio of the reactant/oxidant 41% conversion was obtained which increased to 78% with 1:3 feed ratio. Thereafter increase in the oxidant amount showed no significant change in the conversion. The selectivity of different products also seemed to be affected by the variation in the molar ratio. Selectivity of acetophenone increased from 70% to 88% with increase in the molar ratio from 1:1 to 1:3. Further increasing the oxidant amount (EB:TBHP molar ratio = 1:4) slightly lowered the selectivity to P1. However, under any reaction conditions acetophenone was the major product and the optimum molar ratio would be 1:3.

The better catalytic performance of CZD650 over CZD480 may be correlated to the most reactive crystalline plane exposed on the surface as reflected in the SAED image. As reported by Tsubota and co-workers the increase in the catalytic activity with increase in the calcination temperature may be due to formation of stronger interaction between the two phases of the solid solution (Tsubota et al., 1998). This is also evidenced from the TEM and XRD study. On the other hand, the comparatively reduced activity of CZD800 can be attributed to the degradation of surface area due to sintering of the solid solution as observed from the BET analysis (Table 3). In addition, the electronic properties also vary with the crystallite size owing to the variation in the fraction of the total atoms present in the surface. Sintering of a catalyst may reduce defects in the crystallite much more rapidly than the surface area, thereby decreasing the specific catalytic activity (Carter et al., 1966). The effect of activity and selectivity with

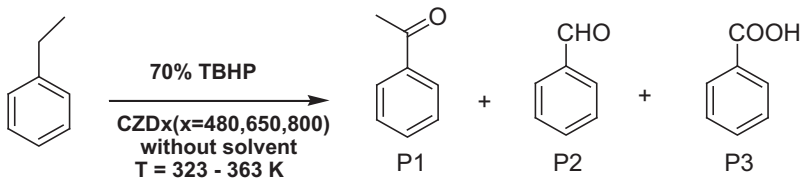

Scheme 2 Reaction pathway for the oxidation of ethyl benzene with TBHP.

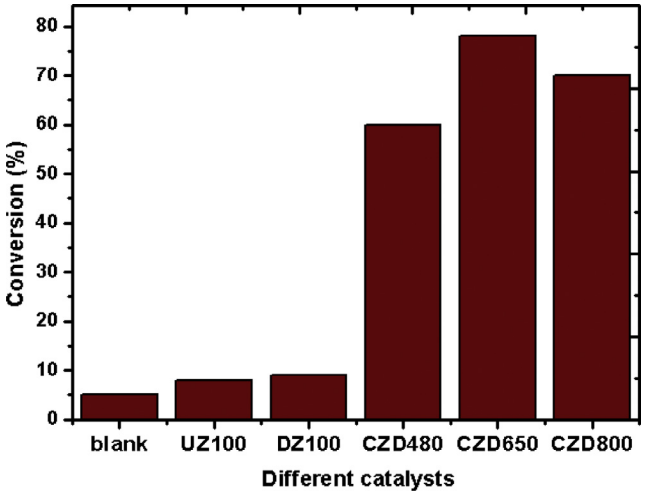

Figure 7 Influence of different catalyst in the oxidation of EB with TBHP. Reaction time = 4 h, EB:TBHP = 1:3, T = 353 K, catalyst amount = 0.1 g.

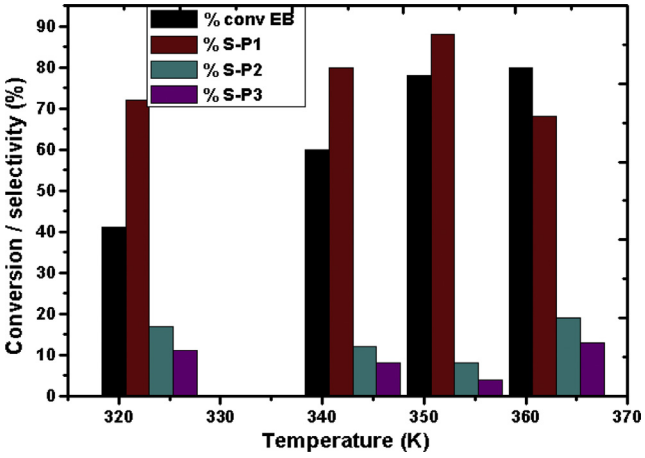

Figure 8 Effect of temperature on the conversion and selectivity over catalyst CZD650. S-P1, S-P2, and S-P3 are respective selectivities of products P1, P2 and P3. Time = 4 h, catalyst amount = 0.1 g, EB:TBHP = 1:3.

Table 4 Effect of different catalysts in the oxidation of EB by TBHP.

Entry	Samples	$EB_{conv.}$ (%)	S-P1 (%)	S-P2 (%)	S-P3 (%)	Refs.
1	Blank	5	62	24	14	This work
2	MMO-0.25/A	54.8 (12 h, 393 K)	79.1	12.9	8.0	Xie et al. (2015)
3	10 VC	20.5 (6 h, 333 K)	72.2	6.7	21.1	Radhika and Sugunan (2007)
4	UZ100	8	63	25	12	This work
5	DZ100	9	65	24	14	-do-
6	CZD480	60	80	12	8	-do-
7	CZD650	78	88	12	8	-do-
8	CZD800	71	85	10	5	-do-
9	CZP480	52	70	19	8	-do-
10	CZP650	66	75	16	4	-do-
11	CZP800	60	74	16	5	-do-

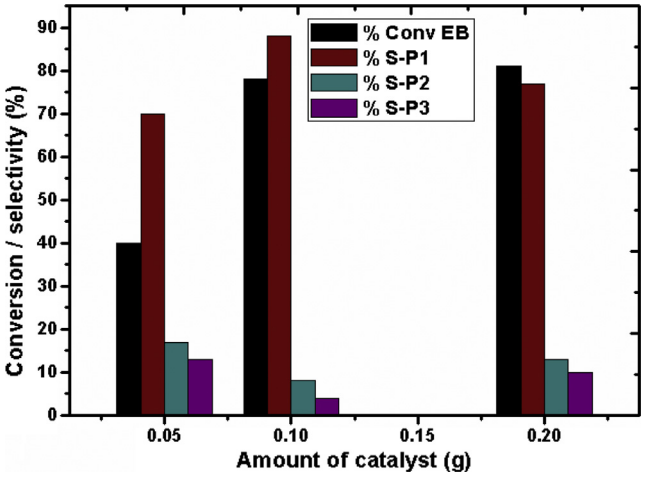

Figure 9 Effect of catalyst amount over catalyst CZD650. Time = 4 h, EB:TBHP = 1:3, T = 353 K.

the variation in the calcination temperature also suggests the existence of different types of reactive sites and the variation in proportion of these sites with crystallite size. James and co-workers reported that the active sites at the corners or edges where crystal faces meet would decrease in proportion to the total sites with the increase in the crystallite size. The varying fraction of edge sites compared to sites on low index planes might also contribute to the observed changes in the catalytic performance (Wu et al., 1975).

In order to investigate the role of the hierarchical topology, controlled experiments were carried out under the optimized conditions with parent MFI loaded CZ (CZP480, CZP650 and CZP800) corresponding to 753, 923 and 1073 K calcination temperatures respectively. The displayed data in Table 4 clearly indicate the enhancement in the conversion and selectivity when alkali treated MFI was used as catalyst support. For an undesilicated MFI zeolite, the majority of the active sites are located inside the micropores; it thus has the shape selectivity dictated by its micropore features only and

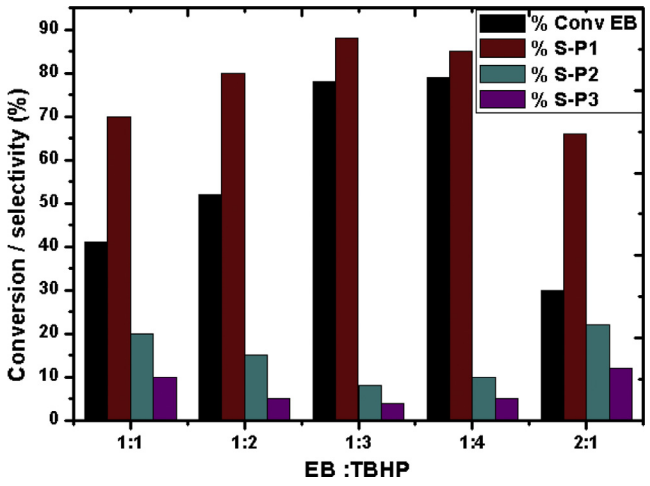

Figure 10 Effect of molar ratio over catalyst CZD650. Time = 4 h, catalyst amount = 0.1 g, T = 353 K.

the reactions mostly take place within these pores. Hierarchical MFI, on the other hand, has a much higher external surface area than conventional (untreated) MFI zeolite due to the reduction in the crystal size. The mesopores formed by the intercrystal spaces are believed to play a major role not only in the diffusion of reactant and products but also in better dispersion of the active sites over the surface. This may help to get better conversion and better selectivity towards desired product. The benefit of Ga containing hierarchical MFI over the parent one for aromatization of propane has recently been published by Ogunronbi et al., 2015. The hierarchical pore arrangement improves the accessibility and shortens the diffusion path length (Li et al., 2009). The large surface area of the desilicated sample and also their enhanced mesopore volume lead to better accommodation of the active sites which helps direct and effective interaction of the reactant with the active site. The activity and selectivity of the reaction correlate well with the crystallite size like that in case of the hierarchical ones.

4.1. Kinetics of the reaction

The kinetics of the reaction was studied for CZD650 catalyst under the optimized condition at different temperature ranges of 323–363 K. A plot of –ln (1- conversion) versus reaction time (Fig. S1) gives a linear relationship with satisfactory R^2 value as displayed in Table 5 indicating the reaction to follow a pseudo-first order dependence. The rate constant at different temperatures was calculated from the slope of the linear fit.

The activation parameters for the overall reaction were calculated by performing the reaction at 353 K with 0.1 g for 4 h with CZD650 catalyst. The activation energy obtained from the Arrhenius equation (Fig. S2) was found to be 21 kJ mol^{-1}. The enthalpy of activation (ΔH) and entropy of the reaction (ΔS) were calculated from the following relations:

$$\Delta H = E_a - nRT \quad (3)$$

$$\Delta S = R\left[\ln A - \ln\left(\frac{kT}{h}\right) - n\right] \quad (4)$$

The enthalpy and entropy of activation were calculated to be 13 kJ mol^{-1} and −264 J mol^{-1} K^{-1} respectively. In addition, compared with other reported catalysts, the CZD650 catalyst behaves in a comparable way or even better in most of the cases, under relatively mild reaction conditions (Lu et al., 2010; Jothiramalingam et al., 2006).

Based upon earlier studies and our experimental data, the oxidation of EB with TBHP was proposed to follow via a free radical mechanism (Dhakshinamoorthy et al., 2009; George and Sugunan, 2008). The active sites of the solid solution could co-ordinate with distant oxygen of TBHP, leading to the generation of tert-butylperoxyl radical (t-BuOO·). This initiated the formation of aryl radical by abstraction of H-atom from EB. Compared with the methyl proton, the methylene proton is more susceptible to oxidation due to the steric reasons of –CH_3 than that in –CH_2–. Moreover the rotation in case of –CH_3 group is more than that of –CH_2–. The activated and co-ordinated oxygen of TBHP reacted with EB to give (1-tert-butoxy ethyl) benzene. The formation of different products follows a competitive pathway. Elimination of tert-butanol/water from (1-tert-butoxy ethyl) benzene led to the formation of acetophenone whereas loss of MeOH yielded benzaldehyde (Jana et al., 2007).

The free radical pathway of the reaction was verified with 2,6-di-tert-butyl-4-methylphenol (BHT). In a particular run under the optimized conditions when the radical scavenger was added, after 4 h the conversion just reached to about 40% (Fig. 11). The GC analysis after prolonged reaction time showed no improvement in the conversion and selectivity. The situation was completely different when compared in the absence of BHT where gradual progress of the reaction was observed with time. All these observed data confirm the reaction to follow free radical mechanism.

4.2. Leaching and reusability

In order to check leaching of CZD650, a fresh reaction was performed and suddenly stopped after 2 h. The GC analysis records a 20% conversion of EB. The catalyst was then removed from the reaction system by simple filtration using Whatman filter paper No. 42 and reaction was continued with the filtrate under similar conditions. Analysis of the mixture after 6 h showed no improvement in the conversion of EB. This assures the absence of leaching and supports the reaction to be purely heterogeneous. This also indicates the strong interaction between the active phase and hierarchical support matrix thereby proving remarkable stability of the catalyst towards oxidation of EB. Recovery and reusability are the two prominent hallmarks for any heterogeneous catalysts. To ensure the reusability of the catalyst the reaction was carried out for 4 h with CZD650 under optimized conditions.

Table 5 Reaction rate constant for the oxidation of EB with TBHP.

Catalyst	Temperature (K)	Rate constant (min^{-1})	R^2
CZD650	323	8.9×10^{-3}	0.96
	343	1.5×10^{-2}	0.97
	353	2.5×10^{-2}	0.98
	363	2.6×10^{-2}	0.96
CZD480	353	2.2×10^{-2}	0.94
CZD800	353	2.4×10^{-2}	0.93

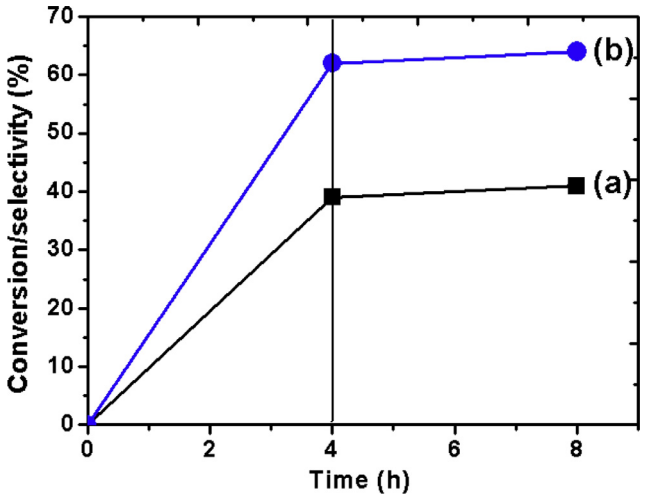

Figure 11 Evidence of free radical mechanism for the oxidation of EB over catalyst CZD650. (a) Conversion of EB with addition of BHT after 4 h and (b) selectivity of acetophenone with addition of BHT after 4 h.

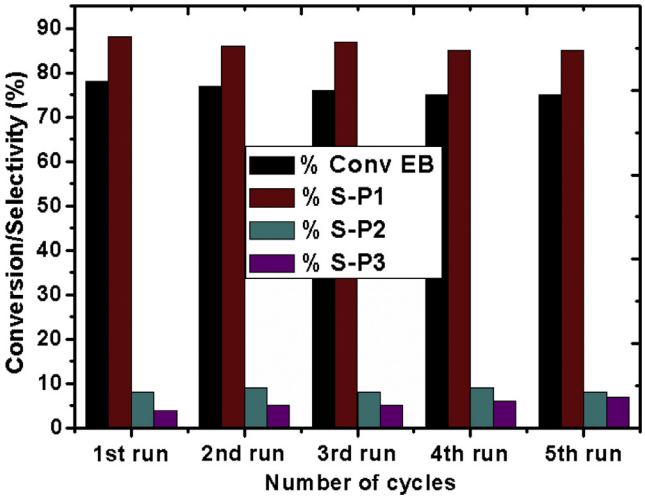

Figure 12 Reusability of the CZD650 catalyst.

The catalyst was then separated from the reaction mixture, washed with acetone and dried. Without further activation the recovered catalyst was tested for fresh reaction mixture of EB and TBHP under the optimized conditions. It is observed that (Fig. 12) CZD650 could maintain its catalytic performance even after the fifth run.

5. Conclusions

An efficient hierarchical MFI loaded ceria–zirconia solid solution has been developed for the oxidation of ethyl benzene to acetophenone using TBHP as the oxidant. The characterization of the synthesized CZ samples showed that the calcination temperature has a direct effect on the morphology, strain and catalytic activity. The catalyst calcined at 923 K exhibits the highest activity for oxidation of EB. The excellent catalytic activity can be attributed to a combination of several factors such as crystallite size, crystallinity, high surface area and hierarchical topology. The catalyst afforded a high yield of acetophenone in a short reaction time without the use of any solvent and can be recycled for several times with retention of its catalytic activity. The present method is convenient, simple and could solve the problems of toxicity, corrosion, waste production and high expenses that are being presently encountered by conventional homogenous catalysts.

Acknowledgements

The authors are grateful to UGC for providing Basic Scientific Research (BSR) fellowship to one of the authors (MN). The authors acknowledge CIF, North Eastern Hill University for TEM analysis and Institute of Advanced Studies in Science and technology (IASST), Boragaon, for XRD analysis. The authors also thank Department of Chemistry and USIC, Gauhati University for extending their support in many relevant measurements associated with the present work.

Appendix A. Supplementary material

Supplementary data associated with this article can be found, in the online version, at http://dx.doi.org/10.1016/j.arabjc.2016.01.010.

References

Alcántara, R., Canoira, L., Joao, P.G., Santosand, J.M., Vázquez, I., 2000. Ethylbenzeneoxidation with air catalysed by bis(acetylacetonate)nickel(II) and tetra-n-butylammonium tetrafluoroborate. Appl. Catal. A. 203, 259–268.

Arshadi, M., Ghiaci, M., 2011. Highly efficient solvent free oxidation of ethylbenzene using some recyclable catalysts: the role of linker in competency of manganese nanocatalysts. Appl. Catal. A 399, 75–86.

Bensalem, A., Muller, J.C., Bozon-Verduraz, F., 1992. From bulk CeO_2 to supported cerium–oxygen clusters: a diffuse reflectance approach. Faraday Trans. 88, 153–154.

Bensalem, A., Bozon-Verduraz, F., Delamar, M., Bugli, G., 1995. Preparation and characterization of highly dispersed silica-supported ceria. Appl. Catal. A 121, 81–93.

Bhoware, S.S., Shylesh, S., Kamble, K.R., Singh, A.P., 2006. Cobalt-containing hexagonal mesoporous molecular sieves (Co-HMS): synthesis, characterization and catalytic activity in the oxidation reaction of ethylbenzene. J. Mol. Catal. A: Chem. 255, 123–130.

Carter, J.L., Cusumano, J.A., Sinfelt, J.H., 1966. Effect of crystallite size on the catalytic activity of nickel. Esso Res. Eng. Co. 70, 2257–2263.

Caicedo-Realpe, R., Perez-Ramirez, J., 2010. Mesoporous ZSM-5 zeolites prepared by a two-step route comprising sodium aluminate and acid treatments. Microporous Mesoporous Mater. 128, 91–100.

Chen, X., Huang, I., Li, Q., 1997. Hydrothermal transformation and characterization of porous silica templated by surfactants. J. Phys. Chem. B 101, 8460–8467.

Colon, G., Valdivieso, F., Pijolat, M., Baker, R.T., Calvino, J.J., Bernal, S., 1999. Textural and phase stability of $Ce_xZr_{1-x}O_2$ mixed oxides under high temperature oxidising conditions. Catal. Today. 50, 271–284.

Corma, A., 1997. From microporous to mesoporous molecular sieve materials and their use in catalysis. Chem. Rev. 97, 2373–2420.

Damyanova, S., Pawelec, B., Arishtirova, K., Huerta, M.V.M., Fierro, J.L.G., 2008. Study of the surface and redox properties of ceria–zirconia oxides. Appl. Catal. A 337, 86–96.

Devika, S., Palanichamy, M., Murugesan, V., 2011. Selective oxidation of ethylbenzene over CeAlPO-5. Appl. Catal. A 407, 76–84.

Dhakshinamoorthy, A., Alvaro, M., Garcia, H., 2009. Metal organic frameworks as efficient heterogeneous catalysts for the oxidation of benzylic compounds with t-butylhydroperoxide. J. Catal. 267, 1–4.
George, K., Sugunan, S., 2008. Nickel substituted copper chromite spinels: preparation, characterization and catalytic activity in the oxidation reaction of ethylbenzene. Catal. Commun. 9, 2149–2153.
Ghiaci, M., Sadeghi, Z., Sedaghat, M.E., Karimi-Maleh, H., Safaei, J., Gil, A., 2010. Preparation of Pd (0) and Pd (II) nanotubes and nanoparticles on modified bentonite and their catalytic activity in oxidation of ethyl benzene to acetophenone. Appl. Catal. A 381, 121–131.
Groen, J.C., Moulijin, J.A., Pérez-Ramírez, J., 2006. Desilication: on the controlled generation of mesoporosity in MFI zeolites. J. Mater. Chem. 16, 2121–2131.
Groen, J.C., Peffer, L.A.A., Moulijin, J.A., Pérez-Ramírez, J., 2004. On the introduction of intracrystallinemesoporosity in zeolites upon desilication in alkaline medium. MicroporousMesoporous Mater. 69, 29–34.
Hu, Y., Yin, P., Liang, T., Jiang, W., Du, Z., Chen, Y., 2008. Microwave-induced synthesis and characterization of nanometer $Ce_{0.5}Zr_{0.5}O_2$ solid solution for the acidic catalytic reaction. Rare metals. 27, 138–141.
Jana, S.K., Kubota, Y., Tatsumi, T., 2007. High activity of Mn–MgAl hydrotalcite in heterogeneously catalyzed liquid-phase selective oxidation of alkylaromatics to benzylic ketones with 1 atm of molecular oxygen. J. Catal. 247, 214–222.
Jothiramalingam, R., Viswanathan, B., Varadarajan, T.K., 2006. Synthesis, characterization and catalytic oxidation activity of zirconium doped K-OMS-2 type manganese oxide materials. J. Mol. Catal. A: Chem. 252, 49–55.
Kalita, B., Talukdar, A.K., 2011. Studies on stability of nanocrystalline MFI zeolite synthesized by a novel method against OH− attack. Mater. Chem. Phys. 129, 371–379.
Kalita, B., Talukdar, A.K., 2009. An efficient synthesis of nanocrystalline MFI zeolite using different silica sources: a green approach. Mater. Res. Bull. 44, 254–258.
Kenevey, K., Valdivieso, F., Soustelle, M., Pijolat, M., 2001. Thermal stability of Pd or Pt loaded Ce0.68Zr0.32O2 and Ce0.50Zr0.50O2 catalyst materials under oxidising conditions. Appl. Catal. B: Environ. 29, 93–101.
Kozlov, A., Kim, D.H., Yezerets, A., Anderson, P., Kung, H.H., Kung, M.F., 2002. Effect of preparation method and redox treatment on the reducibility and structure of supported ceria–zirconia mixed oxide. J. Catal. 209, 417–426.
Li, X., Prins, R., van Bokhoven, J.A., 2009. Synthesis and characterization of mesoporous mordenite. J. Catal. 262, 257–265.
Lu, C., Fu, Z., Liu, Y., Liu, F., Wu, Y., Qin, J., He, X., Yin, D., 2010. A moderate and efficient method for oxidation of ethylbenzene with hydrogen peroxide catalyzed by 8-quinolinolato manganese (III) complexes. J. Mol. Catal. A: Chem. 331, 106–111.
Ogunronbi, K.E., Al-Yassir, N., Al-Khattaf, S., 2015. New insights into hierarchical metal-containing zeolites; synthesis and kinetic modelling of mesoporous gallium-containing ZSM-5 for propane aromatization. J. Mol. Catal. A: Chem. 406, 1–18.
Parida, K.M., Dash, S.S., 2009. Manganese containing MCM-41: synthesis, characterization and catalytic activity in the oxidation of ethylbenzene. J. Mol. Catal. A: Chem. 306, 54–61.
Parra, M.R., Haque, F.Z., 2014. J Aqueous chemical route synthesis and the effect of calcination temperature on the structural and optical properties of ZnO nanoparticles. Mater. Res. Technol. 3, 363–369.
Partenheimer, W., 1995. Methodology and scope of metal/bromide autoxidation of hydrocarbons. Catal. Today. 23, 69–158.
Pérez-Ramírez, J., Christensen, C.H., Egeblad, K., Christensen, C.H., Groen, J.C., 2008. Hierarchical zeolites: enhanced utilisation of microporous crystals in catalysis by advances in material design. Chem. Soc. Rev. 37, 2530–2542.
Perry, R.H., Green, D.W., 1997. Perry's Chemical Engineers' Handbook, seventh ed. McGraw-Hill.
Radhika, T., Sugunan, S., 2007. Vanadia supported on ceria: characterization and activity in liquid-phase oxidation of ethylbenzene. Catal. Commun. 8, 50–56.
Rao, G.R., Sahu, H.R., 2001. XRD and UV-Vis diffuse reflectance analysis of CeO2–ZrO2 solid solutions synthesized by combustion method. Proc. Indian Acad. Sci.(Chem. Sci.). 113, 651–658.
Reddy, B.M., Lakshmanan, P., Bharali, P., Saikia, P., 2006. Dehydration of 4-methylpentan-2-ol over CexZr1−xO2/SiO2nano-composite catalyst. J. Mol. Catal. A: Chem. 258, 355–360.
Reddy, B.M., Lakshmanan, P., 2005. Structural characterization of CeO2−ZrO2/TiO2 and V2O5/CeO2−ZrO2/TiO2 mixed oxide catalysts by XRD, Raman Spectroscopy, HREM, and other techniques. J. Phys. Chem. B 109, 1781–1787.
Reddy, B.M., Ganesh, I., Reddy, E.P., 1997. Study of dispersion and thermal stability of V_2O_5/TiO_2−SiO_2 catalysts by XPS and other techniques. J. Phys. Chem. B 101, 1769–1774.
Singh, P.S., Kosuge, K., Ramaswamyand, K.V., Rao, B.S., 1999. Characterization of MeAPO-11s synthesized conventionally and in the presence of fluoride ions and their catalytic properties in the oxidation of ethylbenzene. Appl. Catal. A 177, 149–159.
Solinas, V., Rombi, E., Ferino, I., Cutrufello, M.G., Colon, G., 2003. Preparation, characterisation and activity of CeO2–ZrO2 catalysts for alcohol dehydration. J. Mol. Catal. A: Chem. 204, 629–635.
Sugiura, M., Ozawa, M., Suda, A., Suzuki, T., Kanazawa, T., 2005. Development of innovative three-way catalysts containing ceria–zirconia solid solutions with high oxygen storage/release capacity. Bull. Chem. Soc. Jpn. 78, 752–767.
Thibault-Starzyk, F., Stan, I., Abelló, S., Bonilla, A., Thomas, K., Fernandez, C., Gilson, J.P., Pérez-Ramírez, J., 2009. Quantification of enhanced acid site accessibility in hierarchical zeolites – the accessibility index. J. Catal. 264, 11–14.
Treacy, M.M.J., Higgins, J.B., 2001. Collection of Simulated XRD Powder Patterns for Zeolite. Elsevier.
Tsubota, S., Nakamura, T., Tanaka, K., Haruta, M., 1998. Effect of calcination temperature on the catalytic activity of Au colloids mechanically mixed with TiO2 powder for CO oxidation. Catal. Lett. 56, 131–135.
Wu, J.C., Harriott, P., 1975. The effect of crystallite size on the activity and selectivity of silver catalysts. J. Catal. 39, 395–402.
Xie, R., Fan, G., Yang, L., Li, F., 2015. Solvent-free oxidation of ethylbenzene over hierarchical flower-like core–shell structured Co-based mixed metal oxides with significantly enhanced catalytic performance. Catal. Sci. Technol. 5, 540–548.